Proceedings of the ASME 2020 15th International Manufacturing Science and Engineering Conference
MSEC2020
June 22-26, 2020, Cincinnati, OH, USA

MSEC2020-7534

ANALYTICAL INVESTIGATION OF VARYING DEFORMATION PATHS USING MICROTUBE INFLATION AND AXIAL TENSION

Elizabeth M. Mamros[1], Brad L. Kinsey
Department of Mechanical Engineering
University of New Hampshire
Durham, NH, USA

Yannis P. Korkolis
Department of Integrated Systems Engineering
The Ohio State University
Columbus, OH, USA

ABSTRACT

Manufacturers invested in a diverse array of industries, ranging from automotive to biomedical, are seeking methods to improve material processing in an effort to decrease costs and increase efficiency. Many parts produced by these suppliers require forming operations during their fabrication. Forming processes are innately complex and involve a multitude of parameters affecting the final part in several ways. Examples of these parameters include temperature, strain rate, deformation path, and friction. These parameters influence the final part geometry, strength, surface finish, etc. Previous studies have shown that varying the deformation path during forming can lead to increased formability. However, a fundamental understanding of how to control these paths to optimize the process has yet to be determined. Adding to the complexity, as the forming process is scaled down for micromanufacturing, additional parameters, such as grain size and microstructure transformations, must be considered.

In this paper, an analytical model is proposed to calculate strain-paths with one or two loading segments and their associated stress-paths. The model is created for investigations of stainless steel 316L using a microtube inflation/tension testing machine. This machine allows for the implementation of two-segment strain-paths through biaxial loading consisting of applied force and internal pressure. The model can be adjusted, based on the desired forming process or available equipment, to output the appropriate parameters for implementation, such as force, displacement, and pressure.

Keywords: non-linear deformation, forming, deformation path, biaxial stress state, micromanufacturing, stainless steel

1. INTRODUCTION

Over the course of the past two decades, research focused on micromanufacturing has been building momentum in an effort to establish a link between macromanufacturing and nanomanufacturing as well as to follow the trend of miniaturization. The latest findings include applications-driven processes including micro-machining, micro-EDM, micro-electrochemical machining, and micro-powder injection molding [1]. As at the macroscale, micro-forming is a high production rate process with exceptional material utilization. In order to achieve high precision and product quality, a fundamental understanding of the processes in addition to accurate prediction models and simulations are needed.

With the decrease in length-scale, a number of new challenges arrive for manufacturers. Assumptions neglecting certain effects in macromanufacturing are no longer valid. Previous studies have shown that material behavior varies significantly at smaller length scales [2-4]. In forming, size-effects occur when a part feature contains < ~10 grains through the thickness and implies that empirical and analytical knowledge derived from the conventional process is not necessarily applicable at the micro-scale [5].

Other factors that may contribute to the difficulty of rescaling a macroscopic manufacturing process include process-material interactions, morphology, mechanical compatibility, equipment resolution, and heat transfer [6]. To fully understand the effects of these parameters and how to control them, further investigations are required.

Whether forming at the micro- or macroscales, the strain paths that the material is subjected to during these operations are typically non-proportional and influence the forming limit curve's (FLC) shape and location. A strain-based FLC is only valid for a material subjected to proportional loading, and thus a

[1] Corresponding Author: emm1109@wildcats.unh.edu

different approach is needed to encompass the entire loading history [7].

Several studies, including Sakash et al. [8], have described methods to construct a stress-based FLC that is independent of deformation and strain path. Yoshida et al. [7] presented an analytical model that considers strain paths with two loading segments and the Marciniak-Kuczynski (M-K) model. It was found that for two linear strain paths with unloading in between the first and second path, the forming limit stresses were path-independent. For the case of two linear strain paths without unloading, the forming limit stresses were highly path dependent. Further experimental validation is required but difficult to achieve since determining the final stress state in experiments is non-trivial [7]. Hence, a path-dependent model coupled with an experimental approach is necessary to more accurately predict the formability and final stress and strain states of materials.

In this paper, an analytical model is presented to determine various loading segment strain-paths and the corresponding stress-paths that can be implemented experimentally to achieve the same final strain state in a micro-forming process. Preliminary results show that although these strain-paths achieve the objective of reaching the same final strain state, the final stress states vary significantly. This may be especially important in applications where the material undergoes plasticity-induced microstructural transformations, e.g., austenite to martensite in SS316L used in this research. The specific application of interest is the fabrication of biomaterials for trauma hardware. For calibration, this model requires initial experiments to be conducted for the material of interest using a microtube inflation/tension machine to create the predicted biaxial stress states. Future experiments will dictate additional modifications to the model to improve the overall accuracy and further validate the analytical results.

2. EXPERIMENTAL SETUP AND METHODS

Biocompatible materials are of interest due to the potential applications of this work. Previous studies were completed using SS304L [9-11], but this investigation utilizes a different low-carbon alloy, SS316L. Similar tube failure experiments were also performed on aluminum 6061 [12-15], although this is not considered to be a biocompatible material. A microtube inflation/tension machine is described and was utilized for the experiments. The analytical model methodology used to determine potential loading segment deformation paths is also outlined in this section. The goal is to create strain-paths with one or two loading segments that achieve the same final strain state (see Fig. 1).

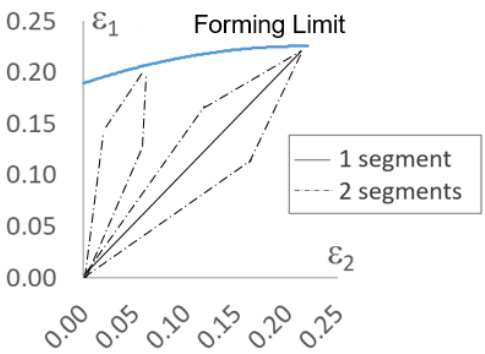

FIGURE 1: Schematic of one and two loading segment deformation paths in biaxial strain space.

2.1 Material

Seamless, fully annealed SS316L microtubes with outer diameter of 2.38 mm and wall thickness of 150 μm were purchased from MicroGroup, part of TE Connectivity [16]. Table 1 shows the chemical properties reported by the manufacturer. The initial microstructure of the material is shown in Fig. 2. Thus, there are approximately 6-8 grains through the thickness in this material, which will directly affect the mechanical behavior (i.e., microforming). Improved microstructural analyses will be completed.

TABLE 1: Chemical composition of SS316L [16]

C%	0.0200
Mn%	1.6400
P%	0.0310
S%	0.0100
Si%	0.3800
N%	0.0430
Ni%	13.1000
Cr%	17.3500
Mo%	2.6400
Fe%	Balance

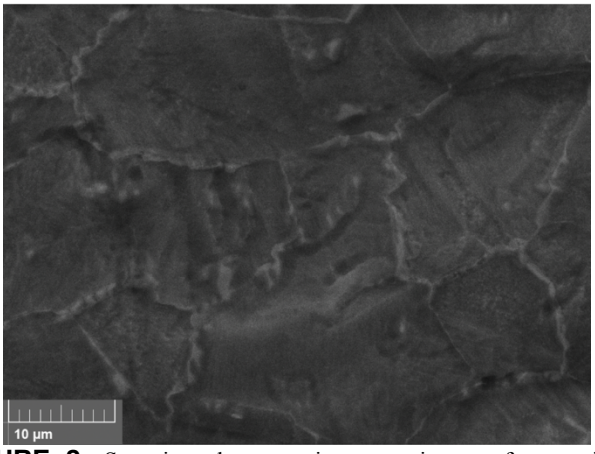

FIGURE 2: Scanning electron microscope image of as-received SS316L microtube.

2.2 Microtube Inflation/Tension Machine

The experiments were conducted on the custom microtube inflation/tension machine shown in Fig. 3 at UNH [9]. This testing machine consists of two major components, a microscale tensile stage from Psylotech and a Teledyne ISCO hydraulic pump, which are coupled via a leader-follower relationship in LabVIEW. The load cell capacity is 2000 N with a resolution of 1 mN, and the maximum displacement is 50 mm with a linear variable displacement transducer resolution of 25 nm. The pump can reach a maximum flow rate of 25 ml/min and a maximum pressure of 138 MPa (20 ksi) with resolutions of ±3% of set point and 138 kPa (20 psi) respectively.

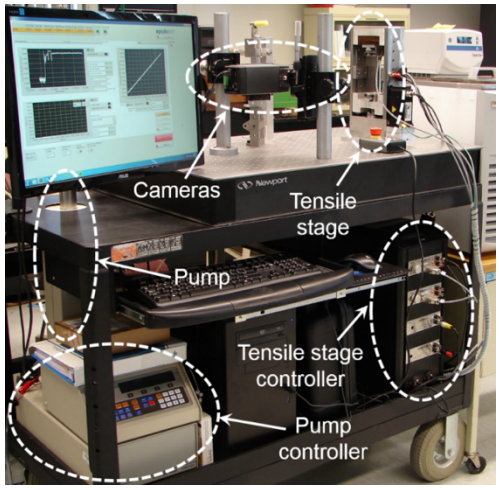

FIGURE 3: Microtube inflation/tension testing machine [10].

The microtube specimen components required assembly (see Fig. 4) prior to being mounted in the custom, 3D printed grips shown in Fig. 4. First, the microtube specimens were cut from the stock tubing, using a Dremel tool, into 64 mm lengths. To prevent the microtube from crimping while tightening the grips, a hollow, metallic insert 17 mm in length was placed in each end creating a 30 mm gage section. Next, the microtube was inserted into the customized glands machined on a lathe out of grade 8 high strength steel to have a through hole and tapered opening at the bottom of the threaded end. Then, 4 conical sleeves (HiP Company) were placed (2 on each end of the specimen) opposite one another as shown in Fig. 4. Lastly, this assembly was inserted into the grips and tightened down. As the custom gland was tightened, the conical sleeves deformed around the microtube securing the specimen and preventing slippage and leakage.

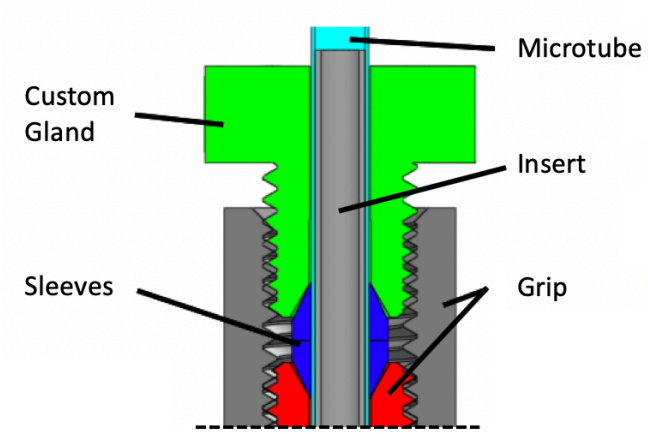

FIGURE 4: Schematic of microtube specimen assembly inside of grip [10].

The stainless steel fluid inlet tube was then attached to the bottom grip, and after purging any air from the system, a plug was inserted into the top grip creating a closed system (see Fig. 5). This specimen preparation procedure follows the methodology used by Ripley and Korkolis [8].

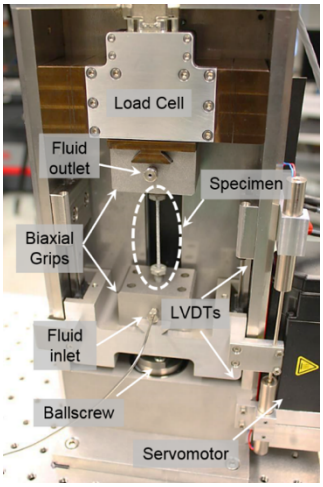

FIGURE 5: Close-up of Psylotech tensile stage with microtube specimen assembly inserted [10].

The microtube inflation/tension machine operates from a customized LabVIEW program. This program maintains a user-specified nominal stress-ratio (i.e., axial:hoop or $\sigma_x{:}\sigma_\theta$) via a leader-follower relationship. The pressure sensor in the system records a measurement and sends this data to the program acting as the leader. The follower component is the tensile stage, which

then receives a signal from the program to apply a load in reaction to the pressure reading thus maintaining the specified stress ratio.

2.3 Digital Image Correlation

Three dimensional Digital Image Correlation (DIC) was utilized to measure the strain field in-situ. Two FLIR 8.9 megapixel cameras were setup (shown in Fig. 3) with 50 mm Schneider Xenoplan compact lenses. Specimens were spray-painted to have a white background with a black speckle pattern. Post processing of the images was completed in VIC-3D from Correlated Solutions, Inc. The DIC parameters include a subset size of 19 and step size of 5, with the area of interest being the entire 30 mm gauge section of the tube. See Fig. 6 for an example strain image from the DIC software a few frames prior to failure showing the localization of strain.

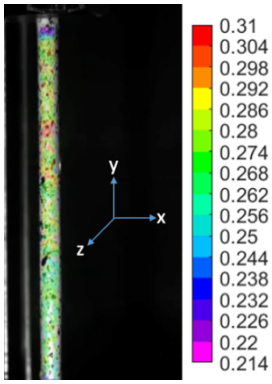

FIGURE 6: Experimental 3D DIC axial strain image.

2.4 Preliminary Experiments

In order to calibrate the analytical model, experimental stress and strain data must be collected for various prescribed single loading segment stress ratios until failure. As an example, data for SS304L is shown for nominal stress-paths with ratios ranging from pure hoop to pure axial (i.e., 0:1 to 1:0) (Fig. 7) and the corresponding induced nominal strain-paths (Fig. 8). The dominant stress dictates the failure mode of the microtube, e.g., if axial stress or hoop stress is greater, the tube will fail axially or circumferentially respectively [10].

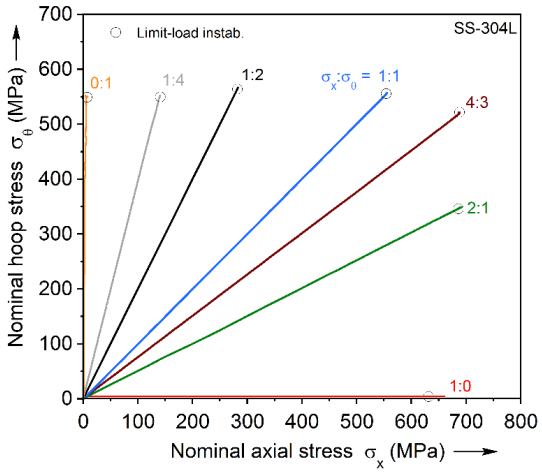

FIGURE 7: Proportional-loading deformation paths for SS304L plotted in stress space [10].

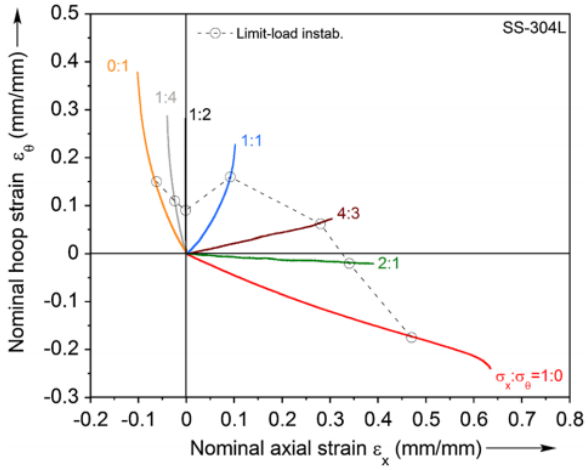

FIGURE 8: Proportional-loading deformation paths for SS304L plotted in strain space [10].

Note that single loading segment stress and strain path data for other stress ratios not shown in Figs. 7 and 8 can also be determined using the microtube inflation/tension machine. Future work will determine these paths for the SS316L material of interest in this research.

2.5 Analytical Model

An analytical model is necessary to determine potential two-loading-segment deformation paths for experimental implementation and was coded in MATLAB. The overall goal of the model is to determine multiple deformation paths that will achieve the same final strain state. Note that the final stress states will vary for the different paths. For simplification of the model, several key assumptions were made. Later modifications, e.g., a more complex yield criterion, will increase the accuracy of the model.

Previous experimental results (see Fig. 8) clearly show that the resulting strain paths from biaxial experiments are non-linear. Therefore, the M-K model [17] was used for the analytical

model to account for this nonlinearity. An imperfection factor (f_o) of 0.995 and step size ($d\varepsilon_{2a}$) of 10^{-5} were selected based on parametric studies. See past publications for equations and implementation details related to the M-K model. Note that while the M-K model is typically used for forming limit diagram failure prediction, here this is simply used to capture the non-linearity of the deformation path which is what causes the localization of the deformation.

Another key assumption was that the material is isotropic and that the von Mises yield criterion characterizes the material well. Preliminary material characterization testing shows that SS316L is slightly anisotropic, so, e.g., a Hill 1948 yield criterion will be added into the model in later versions.

The inputs for the analytical model include the slope of the strain path for the desired path components, material model, and desired final strain state. To create a two loading segment path in the model, two strain paths (see Fig. 8) must be strategically selected from the preliminary experiments. The first step of the analytical model is based purely on mathematics, so the user must recognize unrealistic path combinations via visual inspection of the strain path plot.

For the material model, the Hollomon-Ludwik power law (Eq. 1) is currently coded into the model.

$$\sigma = K \cdot \varepsilon^n \tag{1}$$

The strength coefficient, K, and strain-hardening exponent, n, for our SS316L material are 1310 MPa and 0.39 respectively. Specifically for the microtube inflation/tension model, the specimen center wall radius and wall thickness are also required as inputs, i.e., 1.115 mm and 0.15 mm respectively. Note that for now the strain-paths in Fig. 8, which are for SS304L, are being used while the material model is for SS316L. Future experiments to generate curves for SS316L similar to Fig. 8 will correct this inconsistency.

The analytical model consists of three major steps: 1) determining the transition point between the two loading segments, 2) calculating the microtube inflation/tension force and pressure inputs required to reach the transition point, and 3) calculating the changes in force and pressure required to reach the desired final strain state from the transition point.

In Step 1, the transition point between the two user-specified loading segments and the corresponding point in stress space are calculated. Based on line theory, any two coplanar lines with differing slopes (i.e., not parallel lines) will intersect at exactly one point. Using this theory and the point-slope form of a line:

$$\varepsilon_{2t} = \frac{\varepsilon_{1f} - (m_2 \cdot \varepsilon_{2f})}{m_1 - m_2} \tag{2}$$

where ε denotes the strain path coordinate; m denotes the strain path slope; the subscripts 1, 2 denote major and minor, respectively (where $\varepsilon_{1t} > \varepsilon_{2t}$); and t and f denote transition and final coordinates in strain space. Equation (2) was derived assuming that the specimen starts at a zero strain state. From there:

$$\varepsilon_{1t} = m_1 \cdot \varepsilon_{2t} \tag{3}$$

After incorporating the M-K model to account for non-linearity, Step 1 required slight modifications. Since the initial loading segment, e.g., axial or hoop, is only loaded to small strain values, this path can still be modeled as a "linear" segment. The M-K model only shows significant deviations from the linear paths at large strain values. The actual transition point that would achieve the desired final strain state despite the non-linear, second loading segment was determined iteratively. In addition, the transition point in stress space was linearly adjusted to fall on the known stress path.

In Step 2, the force and pressure values necessary to reach the stress and strain transition points determined in Step 1 are calculated. This requires checking whether hoop or axial stress is the major strain ($\varepsilon_{1t} > \varepsilon_{2t}$) for a given loading segment and whether this changes for the second loading segment. See Fig. 9 where only in Fig. 9b is this change of major versus minor strain required. The remainder of this step is based on solving for stress values based on the M-K model and the methodology described by Sakash *et al.* for converting strain to stress [7].

After obtaining the strain values in Step 1, the corresponding stress values are then calculated assuming von Mises yield criterion. First, the effective strain is determined from:

$$\bar{\varepsilon} = \varepsilon_1 \sqrt{\frac{4}{3}(1 + \rho^2 + \rho)} \tag{4}$$

where ρ, the ratio of minor true strain ε_2 to major true strain ε_1, which is related to α, the ratio of minor true stress $\sigma_2$to major true stress σ_1, by:

$$\alpha = \frac{2\rho + 1}{2 + \rho} \tag{5}$$

Next, the stress values are determined from:

$$\sigma_1 = \frac{K \cdot \bar{\varepsilon}^n}{\sqrt{1 + \alpha^2 - \alpha}} \tag{6}$$

$$\sigma_2 = \alpha \cdot \sigma_1 \tag{7}$$

Regardless of the major and minor strain and stress values, the vertical axis represents hoop stress (Eq. 8) or strain, and the horizontal axis represent axial stress (Eq. 9) or strain as shown in Fig. 9:

$$\sigma_x = \frac{PR_o}{2t_o} + \frac{F}{2\pi R_o t_o} \tag{8}$$

$$\sigma_\theta = \frac{PR_o}{t_o} \tag{9}$$

where P denotes pressure, F denotes axial force applied, R_o denotes the initial radius, and t_o denotes the initial wall thickness.

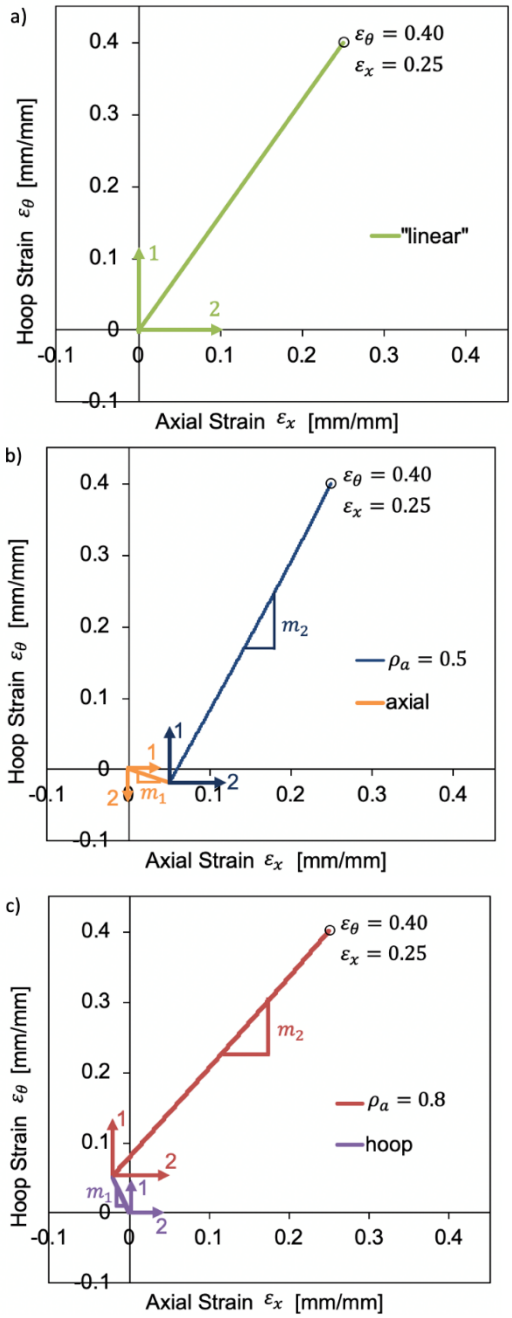

FIGURE 9: Example of reassignment of reference axes according to major and minor principle strains for a) "linear", b) axial-biaxial, c) hoop-biaxial paths.

In Step 3, the strain value differences between the final state and transition point are first determined. Then using these quantities, the methodology of Step 2 is again followed to determine the changes in microtube inflation/tension force and pressure values required to reach the desired final strain state from the transition point.

The outputs of the model include the transition point between the two "linear" loading segments, the stress and strain values for the two loading segments, the desired final strain state, and the axial force and internal pressure values required for the microtube to reach the transition point.

3. RESULTS AND DISCUSSION

The analytical model is currently calibrated to output the force and pressure values necessary to conduct experiments for SS316L using the microtube inflation/tension machine. Dependent upon the application, the user can determine and define a final strain state. One example is depicted in Figs. 10 and 11 for a hoop strain value of 40% and an axial strain of 25%. Note that the individual loading paths are not perfectly "linear" as per Fig. 8. Again, this effect is captured through the M-K model.

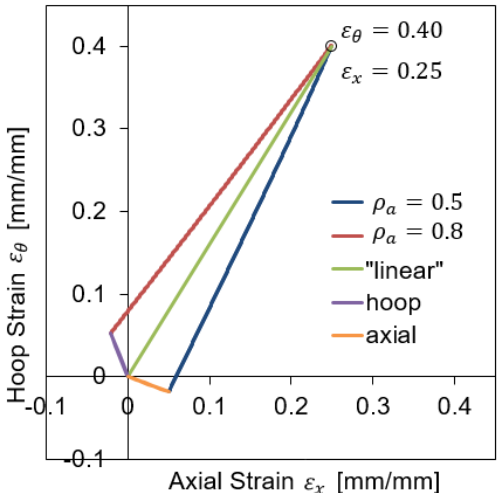

FIGURE 10: Analytically derived, loading segment deformation paths for SS316L achieving the same final strain state.

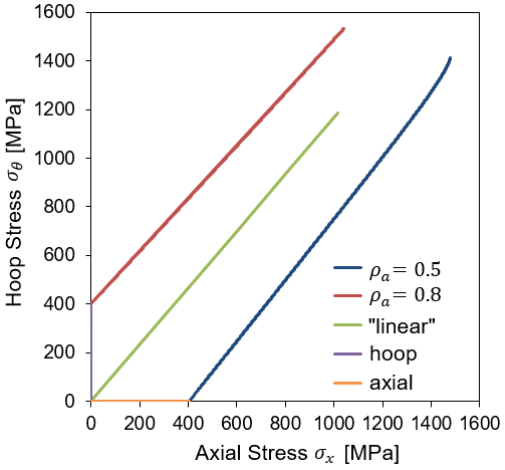

FIGURE 11: Analytically derived, loading segment stress paths for SS316L resulting in differing stress states.

Given the multiple path options outputted by the model, the user can perform additional calculations or optimization algorithms as desired to assist in choosing the most appropriate deformation path for the intended application. In later iterations of the model, some of this functionality may be added to the analytical model.

In terms of micromanufacturing, the different final stress states may offer a diversity of microstructural effects. Specifically for SS316L, the difference in stress states may influence the amount of martensitic transformation and thus the strength of the material in the deformed areas. This could be particularly beneficial in the case of a trauma fixation implant where it is necessary to have increased strength in areas such as the mounting locations.

4. CONCLUSION AND FUTURE WORK

In this paper, an analytical model to determine one- or two-loading-segment deformation paths for SS316L achieving equivalent final strain states utilizing a microtube inflation/tension machine is presented. Preliminary results from proportional loading tests on the aforementioned testing machine were used in the model. Output force and pressure values from the analytical model can be used to implement and validate the deformation paths experimentally. Stress and strain plots representing the deformation paths can also be created from the model. Future iterations of this analytical model will include yield criterion to account for material anisotropy. Continuing experimental determination of the deformation paths using the microtube inflation/tension machine is required.

ACKNOWLEDGEMENTS

Support for the NH BioMade Project is provided by the National Science Foundation through the EPSCoR Research Infrastructure Improvement Award # 1757371. The authors would like to thank Bram Kuijer for the SEM image.

REFERENCES

[1] Qin, Yi (2015) Chapter 1 – Overview of Micro-manufacturing, In Micro and Nano Technologies, Micromanufacturing Engineering and Technology (2nd Edition), William Andrew Publishing, pp. 1-33, ISBN 9780323311496, https://doi.org/10.1016/B978-0-323-31149-6.00001-3.

[2] Lai, X., Peng, L., Hua, P., Lan, S., and Ni, J. (2008) Material behavior modelling in micro/meso-scale forming process with considering size/scale effects. Computational Materials Science, 43, 1003-1009.

[3] Peng, L., Liu, F., Ni, J., and Lai, X. (2007) Size effects in thin sheet metal forming and its elastic plastic constitutive model. Materials and Design, 28, 1731-1736.

[4] Peng, L., Hu, P., Lai, X., Mei, D., and Ni, J. (2009) Investigation of micro/meso sheet soft punch stamping process simulation and experiments. Materials and Design, 30, 783-790.

[5] Razali, Akhtar Razul, Qin, Yi (2013) A Review on Micro-manufacturing, Micro-forming and their Key Issues. Procedia Engineering, Vol. 53, 2013, pp. 665-672, ISSN 1877-7058, https://doi.org/10.1016/j.proeng.2013.02.086.

[6] Ehmann, K. F., Bourell, D., Culpepper, M. L., Hodgson, T. J., Kurfess, T. R., Madou, M., ... & DeVor, R. E. (2005). International assessment of research and development in micromanufacturing. World Technology Evaluation Center Inc., Baltimore, MD.

[7] Yoshida, Kengo; Kuwabara, Toshihiko; and Kuroda, Mitsutoshi. (2007). Path-dependence of the forming limit stresses in a sheet metal. International Journal of Plasticity. 23. 361-384. 10.1016/j.ijplas.2006.05.005.

[8] Sakash, Aaron; Moondra, Sumit; and Kinsey, Brad L. (2006). Effect of yield criterion on numerical simulation results using a stress-based failure criterion. Journal of Engineering Materials and Technology-Transactions of the ASME. 4.

[9] Ripley, P.W. and Korkolis, Y.P. (2016) Multiaxial Deformation Apparatus for Testing of Microtubes Under Combined Axial-Force and Internal-Pressure. Experimental Mechanics 56: 273. https://doi.org/10/1007/s11340-015-0097-y.

[10] Ripley, PW (2014) Biaxial stress testing of SS-304L microtubes by axial load and internal pressure. MS Thesis, Univ. New Hampshire.

[11] Knysh, Paul and Korkolis, Yannis P. (2017). Identification of the post-necking hardening response of rate- and temperature-dependent metals. International Journal of Solids and Structures, Vol. 115–116, pp. 149-160, ISSN 0020-7683, https://doi.org/10.1016/j.ijsolstr.2017.03.012.

[12] Korkolis, Y.P. and Kyriakides, S. (2008) Inflation and burst of anisotropic aluminum tubes for hydroforming applications. International Journal of Plasticity, 24/3, 509-543.

[13] Korkolis, Y.P. and Kyriakides, S. (2008) Inflation and burst of anisotropic aluminum tubes, part II: an advanced yield function including deformation-induced anisotropy. International Journal of Plasticity, 24/9, 1625-1637.

[14] Korkolis, Y.P. and Kyriakides, S. (2009) Path-dependent failure of inflated aluminum tubes. International Journal of Plasticity, 25/11, 2059-2080.

[15] Korkolis, Y.P., Kyriakides, S., Giagmouris, T., Lee, L.-H. (2010) Constitutive modeling of rupture predictions of Al-6061-T6 tubes under biaxial loading paths. Journal of Applied Mechanics - ASME, 064501-1/-5.

[16] TE Connectivity: MicroGroup, Inc. (2019). SS316L Certification of Compliance/Material.

[17] Graf, A. and Hosford, W.F. (1993) Calculations of forming limit diagrams for changing strain paths. W. F. MTA 24:2497. https://doi.org/10.1007/BF02646528.